CAV2021
11th International Symposium on Cavitation
May 10-13, 2021, Daejon, Korea

A water tunnel with inline cyclone separator for removing freestream bubble

Yuhui Lu [1], Omri Ram [2], Jibu Jose [3], Karuna Agarwal [4] and Joseph Katz [*]

Department of Mechanical Engineering, Johns Hopkins University, USA

Abstract: This study explores the possibility of integrating an inline cyclone separator into a research water tunnel as an effective means of continuously reducing the concentration of free-stream bubbles during experiments when large resorbers are not an option, especially in small facilities. The newly built water tunnel in the Laboratory of Experimental Fluid Dynamics at Johns Hopkins University has been developed for refractive-index matched experiments. Experiments aimed at evaluating the cyclone performance are conducted at a velocity of 7.02 m/s in the test section and 4.5 m/s at the inlet to the cyclone. In the first test, an initial dense field of bubbles is created by intentionally cavitating the pump. Then, the pressure is increased and the time evolution of bubble size distribution, with and without the cyclone are compared. In the second experiments, the pressure is reduced to a level that causes pump cavitation while monitoring the evolution of bubble statistics in the test section, also with and without the cyclone. Digital inline holography is used for measuring the spatial distribution of bubbles. During analysis, large ($> 75\,\mu m$) and small bubbles are reconstructed separately using low- & high-pass filtering, and the bubbles are detected using a machine learning based algorithm. In the first experiment, the cyclone accelerates the bubble removal, and effectively eliminates bubbles larger than 60 μm. In the second experiments, the cyclone decreases rate of increase in bubble concentration by nearly 90%, and allows very few bubbles larger than 60 μm through.

Keywords: cyclone separator, bubble removal, water tunnel

1. Introduction

Resorbers, namely large water tanks installed inline in water tunnels to increase the circulation time, have been used for removal/control of bubbles during test involving cavitation [1-2]. This approach is not always feasible for small facilities, where a more compact approach would be preferrable. The present paper describes an effort to utilize a cyclone separator to achieve this goal. Cyclone separators have been widely used for removal of particles in air facilities and gas bubbles in liquid system since its introduction in 1891 [3]. More recently, the mean velocity profile and bubble trajectory have been investigated experimentally [4-5] and numerically [6-8]. These studies show that the peripheral tangential inflow generates a forced vortex in the central part of the cyclone coupled with complex axial and radial velocity distributions. The trajectory and deformation of bubbles in the swirling zone as a function of bubble diameter, Reynolds and Morton numbers have also been investigated using high-speed imaging [9]. However, to the best of our knowledge, this method has never been used as inline removal of bubbles in small research water tunnels. This experimental study describes such an effort, showing that an inline cyclone separator could be used effectively to reduce the concentration of free-stream bubbles or restrict their maximum size. The experimental setup, including the cyclone geometry, is described in the next section, followed by a description of the method used for measuring the freestream bubbles. The results include the time evolution of bubble concentration and their size distributions in the middle of the test section.

* Corresponding Author: Joseph Katz, katz@jhu.edu

Water Tunnel and Cyclone Separator Design

The new water tunnel shown in figure 1(a) has a test section with dimensions of 20.3 x 15.8 x 85 cm^3. The 50 HP pump can generate a maximum speed in the test section of 12.1 m/s with the cyclone and 14.5 m/s bypassing it. The mean pressure in the facility is controlled by a small tank connected to sources of compressed air and a vacuum pump located above the test section. This tunnel has been designed to perform refractive-index matched experiments involving e.g. cavitation, turbulent boundary layers over rough and compliant surfaces, as well as pitching and heaving aerofoils. Matching the refractive index of the fluid, a concentrated aqueous solution of NaI (refractive index $n = 1.493$), with that of acrylic test models and walls, enables unobstructed optical velocity measurements close to complex boundaries. However, in the experiments reported here, the facility contains plain tap water. The bubble removal system consists of a cyclone separator (figure 1b and c) whose top is connected to the abovementioned pressure control tank by a 101 mm diameter flexible pipe. This separator has a diameter of 91.5 cm and height of 152.4 cm tank. The flow enters this tank peripherally from the bottom and exits (also peripherally) from the top. While the inlet and outlet are both standard 30.5 cm diameter pipes, the inlet is throttled by a nozzle aimed at increasing the speed of the inlet wall jet. As the flow swirls upward in the cyclone, the bubbles are driven to the center by the vortex-induced radial pressure gradients, as illustrated in figure 1(b). The bubbles reaching the center are collected by an internal 30.5 cm cone attached to the top of the separator. These bubbles then travel through the flexible pipe to the pressure control tank where they can reach the free surface. Liquid backflow to the cyclone is prevented by extending the pipe to the upper part of the pressure control tank.

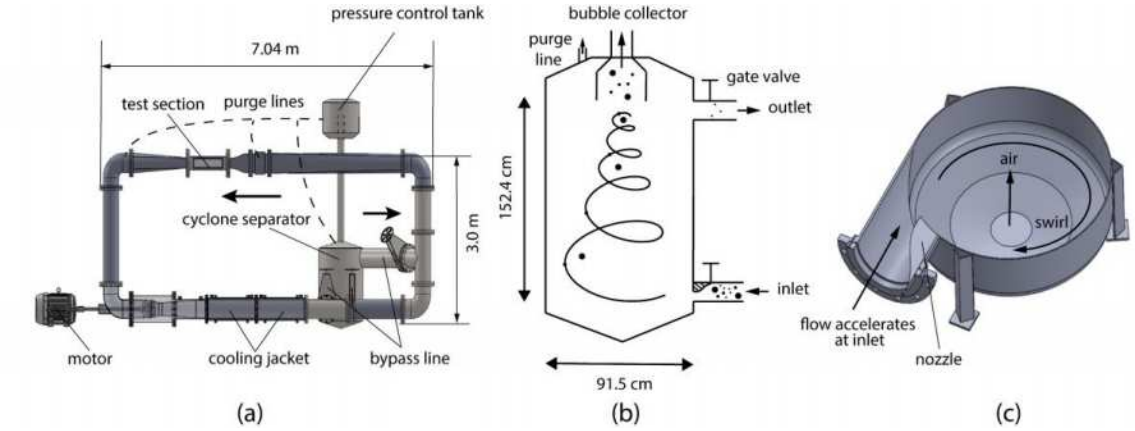

Figure 1. Water Tunnel and Cyclone Separator Design. (a) water tunnel dimension and components, (b) cyclone separator dimension and components, (c) cross section of throttled inlet at bottom of the cyclone.

To obtain a rough estimate of the size of bubbles that are likely to be collected in the center of the cyclone we assume a simplified balance of the radial drag force owing to the bubble migration towards the center and the radial force generated by the pressure gradients in the vortex, namely

$$\frac{1}{2}C_D\rho\pi R^2\left(\frac{dr}{dt}\right)^2 \sim \frac{4}{3}\rho\pi R^3\frac{{V_\theta}^2}{r}$$

Here, r is the radial location of the bubble, R is the bubble radius, C_D is the drag coefficient, and V_θ is the bubble tangential velocity, assumed to be equal to the liquid velocity in a free vortex ($V_\theta \sim 1/r$). This order of magnitude expression does not account for the virtual mass, lift force, and change in bubble radius. Integration of this equation for different inlet speeds indicate that for an inlet velocity of $U_{in} = 4.5\ m/s$ and

* Corresponding Author: Joseph Katz, katz@jhu.edu

the selected tank dimensions, bubbles with diameter larger than 110 μm are expected to migrate to the center of the cyclone and captured by the cone. Increasing the inlet velocity to e.g. 6 m/s, would decrease the entrained diameter to 95 μm. In the present setup, the inlet nozzle is removable and could be readily modified, but the tests reported in this paper have been performed with the abovementioned velocity.

2. Test Procedures and Bubble Detection Method

To evaluate the cyclone efficacy, the experiments have been conducted with and without using the separator. Gate valves installed at the inlet and exit from the cyclone as well as in the main loop enable us to bypass the cyclone in experiments where bubble removal is not a primary concern. Two sets of experiments have been performed at a free-stream velocity of $U_\infty = 7.02\ m/s$ in the test section. In the first experiments, the mean absolute pressure in the test section is intentionally reduced to $p = 47\ kpa$ (cavitation index $\sigma = (p - p_v)/0.5\rho {U_\infty}^2 = 1.78$), causing cavitation in the pump of the water tunnel, which floods the facility with bubbles. Then, the pressure is increased to 77 kpa ($\sigma = 2.99$), which stops the pump cavitation, and the evolution of the freestream bubble concentration and size distribution is measured. In the second experiments, the test section pressure is increased to 112 kpa ($\sigma = 4.42$) until most of the freestream bubbles disappear, and then the pressure is reduced to 57 kpa ($\sigma = 2.18$) while monitoring the increase in freestream bubble concentration. Both experiments have been performed with dissolved oxygen level of 33%, as measured by a Pyroscience Firesting-O2 sensor calibrated using nitrogen-purged (0%) and saturated water (100%).

Digital inline holography [10] is used for measuring the size distribution of freestream bubbles in the center of the test section, as illustrated in figure 2. The light source is a pulsed diode-pumped Nd:YAG laser (Crystal Laser model QL532-500). The beam is spatially filtered and collimated before illuminating the sample volume. In the present setup, the interference patterns are recorded at 2 Hz without any imaging lenses by a 2048 × 2048 pixels CCD camera (PCO 2000), which has a pixel size of 7.4 μm. The cross section of the sample volume is $15.15 \times 15.15\ mm^2$ and it extends across the 203 mm depth of the entire test section.

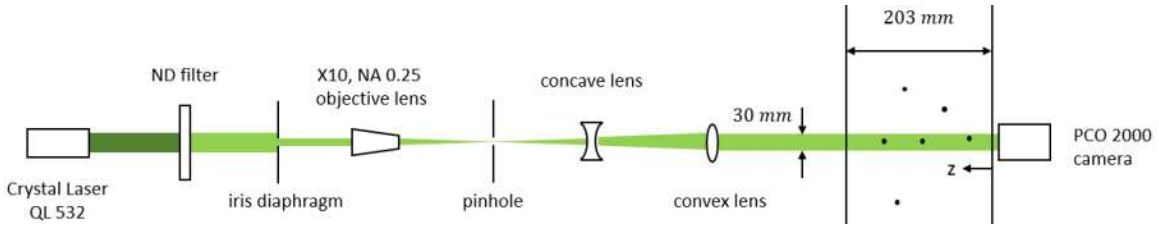

Figure 2. Setup for Digital Inline Holography

The time evolution of bubble statistics has been measured every 30s for 5 min. To process the data, the holograms are enhanced by background subtraction, and then reconstructed using the Rayleigh-Sommerfeld diffraction formula [11]. The inhouse GPU based reconstruction code is described in [12]. The 3D volume containing the bubble images can then be "compressed" to a 2D x-y plane by recording the minimum intensity of each pixel along the z direction. However, this approach has not worked for the present concentrations owing to overlap between images of bubbles located at different depth. To overcome this problem and obtain reliable data especially for small and large bubbles, the reconstruction of small bubbles ($\leq 75\ \mu m$) is separated from that of large bubbles ($> 75\ \mu m$) by high-pass and low-pass filtering of the hologram, respectively, following the steps described in [13]. The resulting data processing diagram, which is illustrated in figure 3(a), consists of the following steps: For small bubble reconstruction,

* Corresponding Author: Joseph Katz, katz@jhu.edu

the original hologram is filtered with a 5th order Butterworth high-pass filter at a cutoff-frequency corresponding to a window size of three times the size of small bubbles. The filtered hologram is numerically reconstructed to obtain the 3D distribution of small bubbles, and then compressed to a plane by recording the minimum intensity for each pixel. For large bubble, the hologram is low-pass filtered at a wavenumber corresponding to half the bubble diameter, and then reconstructed to obtain the 3D intensity field. To prevent overlap of bubbles images located in different depths, the compressed minimum-intensity field is calculated for a series of 5mm thick slabs in z direction, as shown in figure 3(b), and the data in each slab is analyzed separately.

The small bubbles are detected in the compressed image using the machine learning pixel classification algorithm described in [14], which also segments the bubbles and determines their size. For large bubble detection, a 3D machine learning algorithm is utilized to determine in which slab does a bubble come into focus, as illustrated in figure 3(c). The algorithm is trained manually relying on visual detection of in-focus images. It then provides as output the probability that each pixel is part of a focused bubble for each slab, which has a peak in the slab where a bubble comes into focus. The highest probabilities in the z direction are then compressed to a 2D x-y plane. Finally, the abovementioned 2D machine learning algorithm [14] is then used to detect and classify the large bubbles. These procedures have been utilized for all the holograms to obtain the time evolution of bubble size distributions in the facility. A sample processing result using this separate detection method for small and large bubbles is provided in figure 3(d).

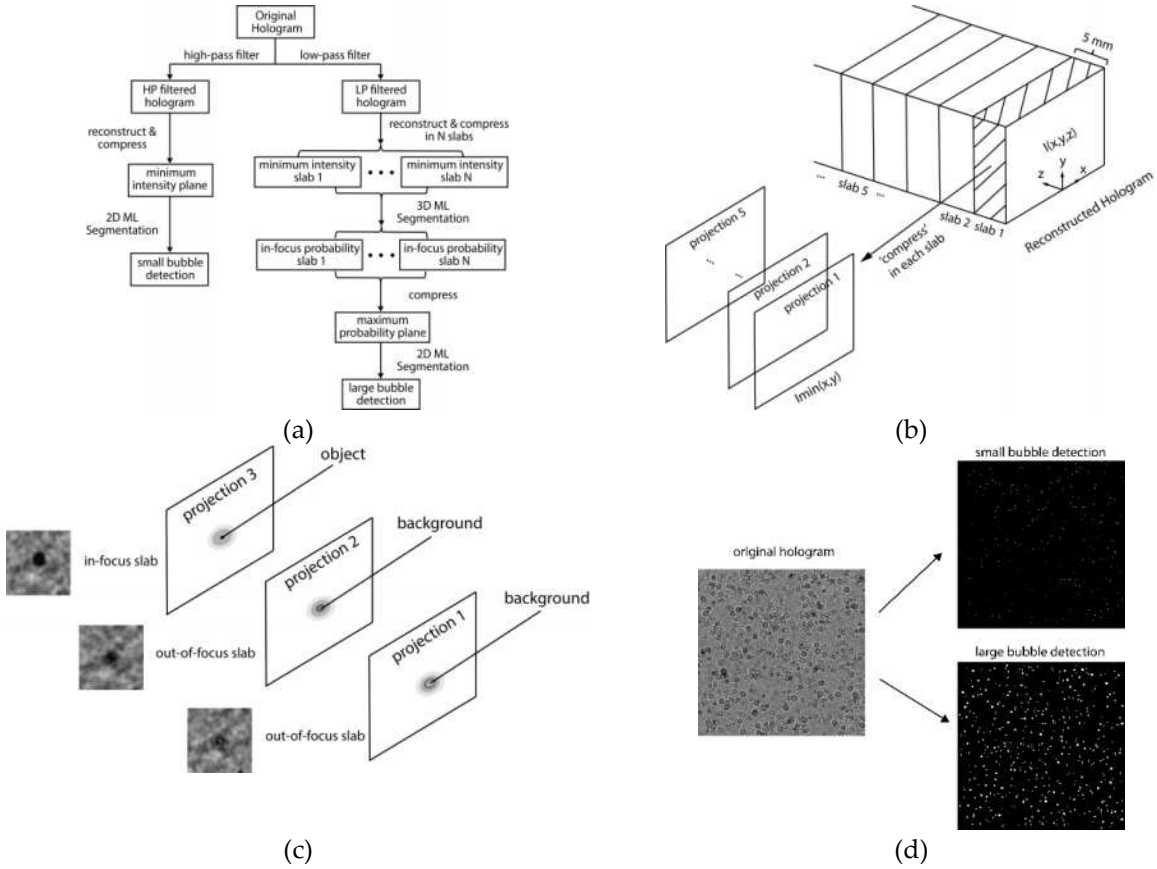

Figure 3. Reconstruction and Machine-Learning Based Detection Procedure. (a) data processing diagram, (b) minimum-intensity compression in slabs for large bubbles, (c) 3D machine learning algorithm, (d) data processing result of a sample hologram.

* Corresponding Author: Joseph Katz, katz@jhu.edu

3. Results and Discussions

Figure 4(a) shows the time evolution of total air volume $V_{air}(t)$ at the specified time, normalized by the initial volume at the beginning of each experiment $V_{air}(t_0)$, for the first experiment. As is evident, the decay rate of gas volume with the cyclone is 50% higher than that without the cyclone, hence after 3 min the gas volume with the cyclone is seven times smaller than that without one. Figure 4(b) and (c) shows the bubble size distributions at the beginning and the end of the test, respectively. Furthermore, the size distribution of air bubble at $t = 5\ min$ presented in Figure 4(c) shows that all the bubbles with diameter larger than 60 μm have been removed by the cyclone. This cutoff size is 45% smaller than the predicted minimum size of captured bubbles (110 μm).

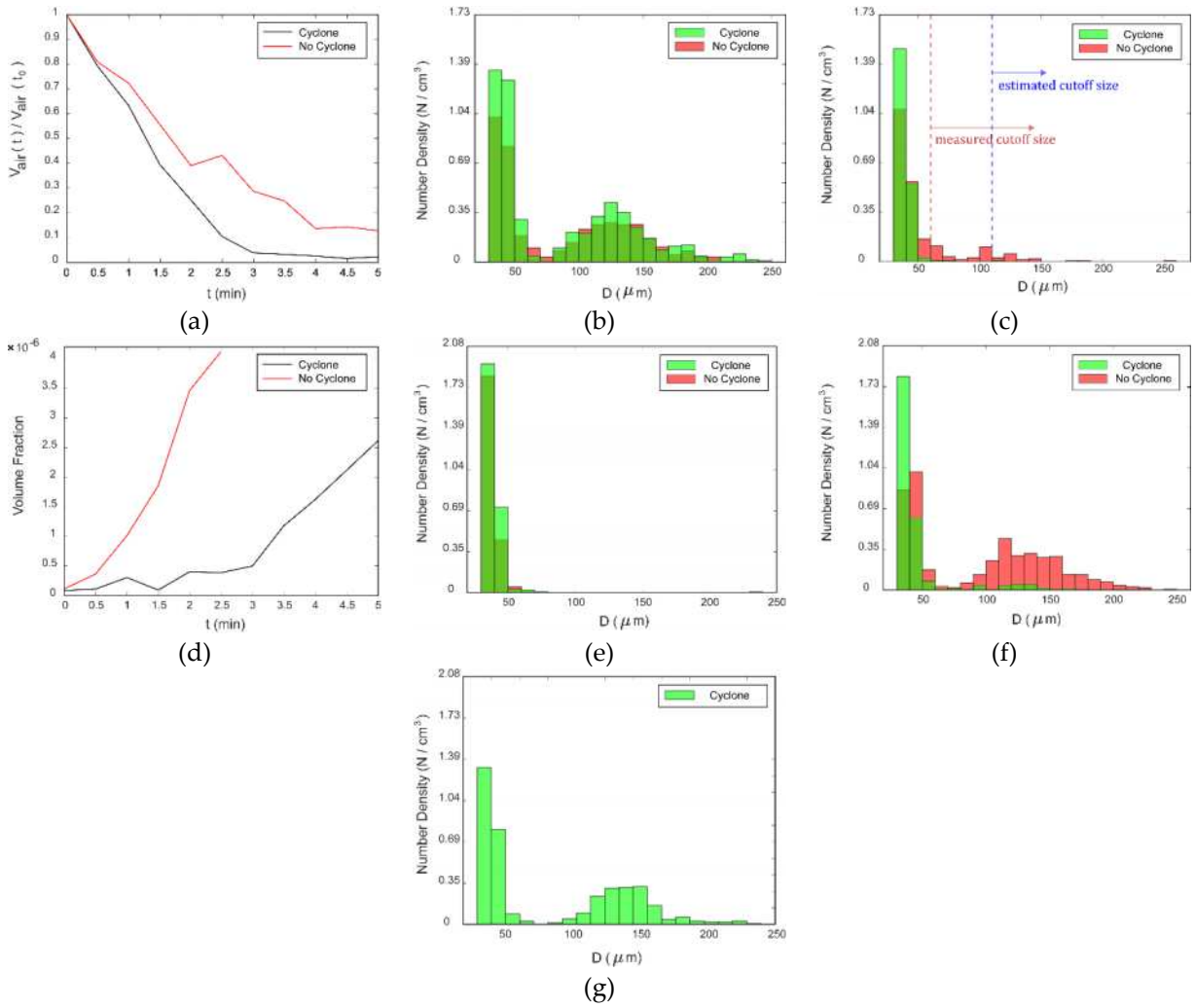

Figure 4. Statistics of bubble concentration evolution at $U_{in} = 4.5\ m/s$. (a)-(c) the first experiment measuring decay rate of bubble concentration, (d)-(g) the second experiment measuring increase rate of bubble concentration. (a) evolution of bubble concentration in the first experiment, (b) bubble size distribution at $t = 0$, (c) bubble size distribution at $t = 5\ min$, (d) evolution of bubble concentration in the second experiment, (e) bubble size distribution at $t = 0$, (f) bubble size distribution at $t = 2.5\ min$, (g) Bubble size distribution at $t = 5\ min$.

* Corresponding Author: Joseph Katz, katz@jhu.edu

For the second experiment, which involves a decrease in pressure, Figure 4(d) shows the time evolution of volume fraction of air, i.e. the total volume of the bubbles divided by the volume covered by the holograms. Figure 4(e) and (f) shows the bubble size distributions at the beginning of the test and after 2.5 min, respectively. While the initial void fractions are very similar, after 2.5 min, the bubble void fraction without a cyclone is ten times higher than that with the cyclone. In fact, without the cyclone the flow becomes so flooded with bubbles after 3 min owing to pump cavitation that individual bubbles can no longer be resolved by holograms. After 2.5 min, figure 4(f) shows that the number of bubbles with diameter larger than 60 μm with a cyclone is ten times smaller than that without cyclone, indicating that most of the larger bubbles are removed. Later, the bubble concentration keeps on increasing, and in fact accelerating, resulting in the size distribution after 5 min presented in figure 4(g).

4. Conclusions

The present study tests the effect of using inline cyclone separator as an alternative mean to remove freestream bubbles from the flow in a small research water tunnel. The bubble size distributions are measured using digital inline holography combined with machine learning based data analysis. For a separator with a predicted cutoff size of 110 μm, based on a simplified model, the experiments indicate that most of the bubbles larger than 60 μm are effectively removed. Better predictions would require a more accurate model for the bubble dynamics accounting for e.g. virtual mass, lift force, mass diffusion, changes to the bubble size owing to variations in pressure, and more accurate description of the flow field in the cyclone. Even when the facility is continuously flooded with bubbles by pump cavitation, the separator still removes most of them, at least for a while. This approach can be readily adapted for degassing small facilities.

Acknowledgments: Construction of the new water tunnel and the cyclone as well as the research described in this paper have been funded by the Office of Naval Research under grant numbers N00014-19-1-2096 and N00014-18-1-2635. Gregory Orris and Ki-Han Kim are the program Officers.

References

1. Calmon M, Farhat M, Fua P, et al. L'hydroptere: How multidisciplinary scientific research may help break the sailing speed record. Proceedings of the 2nd international conference on innovation in high performance sailing yachts. RINA, 2010.
2. Brandner, P. A., Lecoffre, Y., & Walker, G. J. Development of an Australian national facility for cavitation research. 6th International symposium on cavitation. 2006.
3. Bretney, E., 1891, Water Purifier, U.S. Patent, No. 543-105.
4. Peng W, Hoffmann A C, Boot P, et al. Flow pattern in reverse-flow centrifugal separators. Powder Technology, 2002, 127(3): 212-222.
5. Hreiz R, Gentric C, Midoux N, et al. Hydrodynamics and velocity measurements in gas–liquid swirling flows in cylindrical cyclones. Chemical engineering research and design, 2014, 92(11): 2231-2246.
6. Jiang L, Liu P, Zhang Y, et al. The effect of inlet velocity on the separation performance of a two-stage hydrocyclone. Minerals, 2019, 9(4): 209.
7. Wang B, Xu D L, Chu K W, et al. Numerical study of gas–solid flow in a cyclone separator. Applied Mathematical Modelling, 2006, 30(11): 1326-1342.
8. Elsayed K, Lacor C. The effect of cyclone inlet dimensions on the flow pattern and performance. Applied mathematical modelling, 2011, 35(4): 1952-1968.

* Corresponding Author: Joseph Katz, katz@jhu.edu

9. Zhang T, Qian Y, Yin J, et al. Experimental study on 3D bubble shape evolution in swirl flow. Experimental Thermal and Fluid Science, 2019, 102: 368-375.
10. Schnars U, Jüptner W P O. Digital recording and numerical reconstruction of holograms. Measurement science and technology, 2002, 13(9): R85.
11. Katz J, Sheng J. Applications of holography in fluid mechanics and particle dynamics. Annual Review of Fluid Mechanics, 2010, 42: 531-555.
12. Wang, Jin. Impact of Pressure on Deformation of a Compliant Wall in a Turbulent Boundary Layer. Diss. Johns Hopkins University, 2019.
13. Li C, Miller J, Wang J, et al. Size distribution and dispersion of droplets generated by impingement of breaking waves on oil slicks. Journal of Geophysical Research: Oceans, 2017, 122(10): 7938-7957.
14. Berg S, Kutra D, Kroeger T, et al. Ilastik: interactive machine learning for (bio) image analysis. Nature Methods, 2019, 16(12): 1226-1232.

* Corresponding Author: Joseph Katz, katz@jhu.edu